GENERALIZED THERMOELASTIC WAVES IN CYLINDERS
DUE TO LOCALIZED HEATING

Hao Bai, Ravi Chitikireddy, Arvind H. Shah and Subhendu K. Datta

■
■■msp

GENERALIZED THERMOELASTIC WAVES IN CYLINDERS
DUE TO LOCALIZED HEATING

HAO BAI, RAVI CHITIKIREDDY, ARVIND H. SHAH AND SUBHENDU K. DATTA

This paper presents a theoretical study of propagation of thermoelastic waves generated by concentrated heating of the outer surface of circular cylindrical shells. The generalized thermoelastic theory proposed by Lord and Shulman is used to model the response of a circular cylindrical shell to a pulsed laser focused on the surface of the cylinder. Guided wave modes in the cylinder are obtained by a semianalytical finite element method. Dynamic response is constructed numerically by superposition of guided wave modes. In this method, the cylinder is discretized in the radial direction into several coaxial circular cylinders (subcylinders) and the radial dependence of the displacement and temperature in each subcylinder is approximated by quadratic interpolation polynomials. Numerical results for the variation through the thickness of various physical quantities of interest at a location away from the source are presented for a silicon nitride (Si_3N_4) tube for illustration purposes. The frequency dependence of the response quantities is discussed and attention is focused on convergence and accuracy of the computed results.

1. Introduction

Laser-based ultrasonic techniques have been used in several recent studies to generate elastic waves in solids. These techniques provide a number of advantages over conventional ultrasonic methods, such as higher spatial resolution, noncontact generation and detection of waves, and the ability to operate on curved and rough surfaces [Scruby and Drain 1990]. The use of generalized thermoelasticity theories to analyze thermoelastic waves generated by a pulsed laser beam has received some attention in recent years. The classical theory of heat conduction in solids treats the flux of heat as proportional to the gradient of temperature in the media. Thus, the heat conduction equation is a parabolic partial differential equation, which predicts an infinite thermal wave speed. This assumption of infinite speed of heat propagation is contrary to physical reality. To rectify this paradox, several generalizations to the classical heat conduction equation and the thermoelastic wave equations have been proposed. These generalizations take into account the finite wave speed of the thermal pulse travelling through the body.

Lord and Shulman [1967] presented a generalized theory of thermoelasticity for an isotropic body that was a modification of the Fourier law of heat conduction by the inclusion of a relaxation time. This then predicts a finite thermal wave speed. Other generalizations were proposed by Green and Lindsay [1972], who developed a temperature-rate dependent theory that included two relaxation times, and by Green and Naghdi [1993], who introduced a thermoelasticity theory without energy dissipation. See [Ignaczak and Ostoja-Starzewski 2010] for a theoretical development of thermoelasticity with finite wave speeds.

Guided surface (Rayleigh) waves and Rayleigh–Lamb waves in plates have been studied by several investigators using generalized thermoelasticity theories. Rayleigh–Lamb waves in plates using Lord–Shulman theory have been discussed in [Datta and Shah 2009]. References to many other works can be found in [Sharma et al. 2000; Verma and Hasebe 2001; Verma 2002; Al-Qahtani and Datta 2004; Al-Qahtani et al. 2005]. Compared to many studies that have dealt with plates, there is a very limited amount of reported work on waves in cylinders using generalized thermoelastic theories.

Dispersion of longitudinal thermoelastic wave propagation in a circular isotropic cylinder was studied by Erbay and Şuhubi [1986], who considered the cylinder surface to be stress-free and at a constant temperature. Elnagar and Abd-Alla [1987] studied the influence of the initial stress on Rayleigh wave propagation in a generalized thermoelastic cylinder. Three-dimensional vibration of a homogeneous transversely isotropic thermoelastic cylindrical panel was investigated in [Sharma 2001; Sharma and Sharma 2002]. Recently, wave propagation in a thermoelastic cylinder of an arbitrary cross section was reported by Ponnusamy [2007], who used a collocation method to study the dispersive waves.

Circumferential isothermal elastic waves in an isotropic cylinder generated by a laser pulse and their scattering by a surface defect was studied experimentally in [Clorennec and Royer 2003]. Pan et al. [2004; 2006] investigated theoretically and experimentally the isothermal acoustic waves generated by a laser point pulse in an isotropic and a transversely isotropic cylinder. Three-dimensional Fourier transforms were used to find the dynamic displacements at the cylinder surface.

In this work, we present an analysis of generalized thermoelastic waves in cylinders due to a pulsed laser beam focused on the surface of the cylinders. The generalized heat conduction theory of [Lord and Shulman 1967] has been adopted here. A semianalytical finite element (SAFE) method was employed earlier in [Chitikireddy et al. 2010] to obtain the dispersion relations for guided thermoelastic waves in free cylinders. These modes are used here to represent the time-harmonic solutions for the field quantities due to the laser excitation. Based on this solution, the steady-state Green's function for the thermoelastic cylinder can also be constructed. Zhuang et al. [1999] used the SAFE method to study the steady-state Green's function for isothermal composite cylinders. The response in the time domain can be obtained by applying an inverse Fourier transform. Here, the distributions of the stresses, displacements, and heat flux through the thickness of the cylinder are presented at certain chosen frequencies to show the convergence of the results.

2. Formulation

2.1. *Governing equations.*

Consider an infinite thermoelastic cylinder of inner radius r_i and outer radius r_o in the cylindrical coordinate system (r, θ, z) with the origin at the centre of the cross section of the cylinder as shown in Figure 1. The generalized Lord–Shulman governing equations of thermoelasticity, in the presence of a body force and heat source, are given by [Al-Qahtani et al. 2005]

$$\sigma_{ij,j} + f_i = \rho \ddot{u}_i, \quad T_0 \rho \dot{\eta} + Q = -q_{i,i}, \quad \sigma_{ij} = C_{ijkl}\varepsilon_{kl} - \beta_{ij}T,$$
$$\rho \dot{\eta} = \beta_{ij}\dot{\varepsilon}_{ij} + \frac{\rho c_E}{T_0}\dot{T}, \quad q_i + \tau_0 \dot{q}_i = -k_{ij}T_{,j}. \tag{1}$$

The physical quantities and material constants appearing in these equations are: σ_{ij}, the components of the stress tensor; u_i, the components of the displacement; ε_{ij}, the components of the strain tensor; C_{ijkl}, the elastic constants; q_i, the components of the heat flux vector; ρ, the mass density; T_0, the

reference temperature; η, the entropy density; T, the temperature change; c_E, the specific heat at constant deformation; τ_0, the thermal relaxation time; β_{ij}, the thermal coefficients; k_{ij}, the coefficients of thermal conductivity; f_i, the body force per unit volume; and Q, the heat source. In the above equations, a superposed dot indicates the derivative with respect to time.

We define nondimensional quantities

$$r_i^* = \frac{r_i}{H}, \quad u_i^* = \frac{u_i}{\delta H}, \quad T^* = \frac{T}{\bar{T}}, \quad t^* = \frac{\bar{v}}{H}t, \quad \sigma_{ij}^* = \frac{\sigma_{ij}}{\delta \bar{c}}, \quad q_i^* = \frac{q_i}{\bar{q}}, \quad \varepsilon_{ij}^* = \frac{\varepsilon_{ij}}{\delta},$$

$$\rho^* = \frac{\rho}{\bar{\rho}}, \quad c_E^* = \frac{c_E}{\bar{c}_E}, \quad \beta_{ij}^* = \frac{\beta_{ij}}{\bar{\beta}}, \quad k_{ij}^* = \frac{k_{ij}}{\bar{k}}, \quad c_{ijkl}^* = \frac{c_{ijkl}}{\bar{c}}, \quad \tau_0^* = \frac{\bar{v}}{H}\tau_0, \quad T_0^* = \frac{T_0}{\bar{T}}, \tag{2}$$

where

$$\bar{v} = \sqrt{\frac{\bar{c}}{\bar{\rho}}}, \quad \delta = \sqrt{\frac{\bar{k}\bar{T}}{H\bar{v}\bar{c}}}, \quad \bar{q} = \frac{\bar{k}\bar{T}}{H}, \quad \bar{\beta} = \frac{\delta\bar{c}}{\bar{T}}, \quad \bar{c}_E = \frac{\bar{k}}{\bar{\rho}\bar{v}H}. \tag{3}$$

In the sequel, two more nondimensional quantities are defined: the wave number $k^* = kH$ and frequency $\omega^* = \omega H/\bar{v}$. Here $\bar{\rho}, \bar{k}, \bar{c}, H,$ and $\bar{T}$ are the basic normalization quantities, and the rest can be derived from them as shown above. Note that $\bar{\rho}, \bar{k}, \bar{c},$ and $\bar{T}$ can be taken suitably depending upon the material properties of the cylinder. This nondimensionalization scheme yields all dimensionless equations in the same form as their dimensional counterparts. Therefore, this normalization could be used to solve multilayer structures.

Using (1), the governing coupled thermoelastic equations can be written as

$$c_{ijkl}u_{k,lj} - \beta_{ij}T_{,j} + f_i = \rho\ddot{u}_i, \qquad \left(1 + \tau_0\frac{\partial}{\partial t}\right)[T_0\beta_{ij}\dot{\varepsilon}_{ij} + \rho c_E\dot{T} + Q] = k_{ij}T_{,ij}. \tag{4}$$

Writing these equations in terms of the nondimensional quantities defined in (2) and introducing

$$f_i^* = \frac{H}{\delta\bar{c}}f_i, \quad Q^* = \frac{H^2}{\bar{k}\bar{T}}\left(1 + \tau_0^*\frac{\partial}{\partial t^*}\right)Q,$$
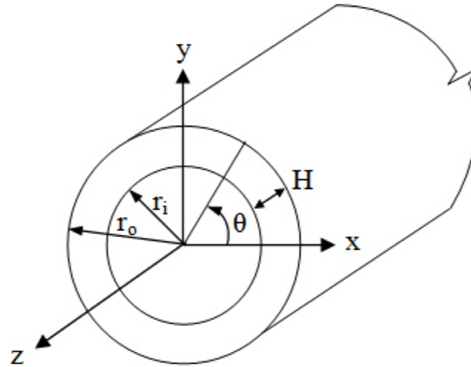
Figure 1. Geometry of the cylinder.

we obtain

$$c_{ijkl}^* u_{k,lj}^* - \beta_{ij}^* T_{,j}^* + f_i^* = \rho^* \ddot{u}_i^*,$$

$$\beta_{ij}^* T_0^* \left(1 + \tau_0^* \frac{\partial}{\partial t^*}\right) \dot{u}_{i,j}^* - k_{ij}^* T_{,ij}^* + \rho^* c_E^* \left(1 + \tau_0^* \frac{\partial}{\partial t^*}\right) \dot{T}^* = -Q^*. \tag{5}$$

These two equations have to be solved by numerical techniques for a generally anisotropic medium. If the material of the cylinder is transversely isotropic with the symmetry axis coinciding with the z-axis, the equations can be solved analytically in terms of Bessel functions. This will be discussed in a future publication. In the following, we will use the SAFE method to solve the problem. For convenience, the superscript * will be dropped.

2.2. *Semianalytical finite element formulation.*

In this method, the radial dependence of the displacement u and the temperature T are approximated by one-dimensional isoparametric finite elements. The total thickness of the cylinder H is composed of cylindrical layers and each layer can have distinct thermoelastic properties and thickness. By using the SAFE method, the thickness of the cylinder is discretized into N laminas. Quadratic interpolation polynomials are used to approximate the displacement and temperature field over each lamina in the radial direction.

The displacement and temperature of the k-th lamina are expressed as

$$\begin{aligned} u(r, \theta, z, t) &= N_1(\xi) u^e(\theta, z, t), \\ T(r, \theta, z, t) &= N_2(\xi) T^e(\theta, z, t), \end{aligned} \tag{6}$$

with

$$r = N_2(\xi) R^e. \tag{7}$$

Here

$$N_1(\xi) = \begin{bmatrix} n_1 & 0 & 0 & n_2 & 0 & 0 & n_3 & 0 & 0 \\ 0 & n_1 & 0 & 0 & n_2 & 0 & 0 & n_3 & 0 \\ 0 & 0 & n_1 & 0 & 0 & n_2 & 0 & 0 & n_3 \end{bmatrix}, \quad N_2(\xi) = \begin{bmatrix} n_1 & n_2 & n_3 \end{bmatrix}, \tag{8}$$

$$u^e = (u_{r1}, u_{\theta 1}, u_{z1}, u_{r2}, u_{\theta 2}, u_{z2}, u_{r3}, u_{\theta 3}, u_{z3})^T, \quad T^e = (T_1, T_2, T_3)^T, \quad R^e = (R_b, R_m, R_f)^T. \tag{9}$$

In (8), the shape functions are

$$n_1 = \tfrac{1}{2}\xi(\xi - 1), \quad n_2 = 1 - \xi^2, \quad n_3 = \tfrac{1}{2}\xi(\xi + 1), \quad -1 \leq \xi \leq 1. \tag{10}$$

In (9) the nodal displacements u_{rj}, $u_{\theta j}$, and u_{zj} and temperature T_j, where $j = 1, 2, 3$, are taken at the inner surface ($r = R_b$), middle layer ($r = R_m = (R_b + R_f)/2$), and outer surface ($r = R_f$) of the k-th lamina.

The strain tensor and temperature gradient are expressed as

$$\varepsilon = D_1 u^e + D_2 u_{,\theta}^e + D_3 u_{,z}^e, \quad T' = B_1 T^e + B_2 T_{,\theta}^e + B_3 T_{,z}^e. \tag{11}$$

The matrices B_1, B_2, B_3, D_1, D_2, and D_3 are defined in the Appendix. The stress vector is given by

$$\sigma = C(D_1 u^e + D_2 u_{,\theta}^e + D_3 u_{,z}^e) - \beta N_2 T^e. \tag{12}$$

The variational principle of thermoelasticity [Al-Qahtani et al. 2005] is

$$\int_{t_0}^{t_1} \int_V \left(\delta \boldsymbol{\varepsilon}^T \boldsymbol{\sigma} - \delta \boldsymbol{T'}^T \boldsymbol{K} \boldsymbol{T'} - \delta \boldsymbol{T'}^T (\boldsymbol{q} + \tau_0 \dot{\boldsymbol{q}})\right) dV \, dt = \int_{t_0}^{t_1} \int_V (\boldsymbol{f} - \delta \boldsymbol{u}^T \rho \ddot{\boldsymbol{u}}) \, dV \, dt. \tag{13}$$

The first term on the left-hand side is

$$\int_{t_0}^{t_1} \int_V \delta \boldsymbol{\varepsilon}^T \boldsymbol{\sigma} \, dV \, dt = \int_{t_0}^{t_1} \int_V (\boldsymbol{D}_1 \delta \boldsymbol{u}^e + \boldsymbol{D}_2 \delta \boldsymbol{u}^e_{,\theta} + \boldsymbol{D}_3 \delta \boldsymbol{u}^e_{,z})^T [\boldsymbol{C}(\boldsymbol{D}_1 \boldsymbol{u}^e + \boldsymbol{D}_2 \boldsymbol{u}^e_{,\theta} + \boldsymbol{D}_3 \boldsymbol{u}^e_{,z}) - \boldsymbol{\beta} \boldsymbol{N}_2 \boldsymbol{T}^e] \, dV \, dt$$

$$= \int_{t_0}^{t_1} \int_z \int_\theta \delta u^{eT} \begin{bmatrix} \boldsymbol{K}_{11} \boldsymbol{u}^e + (\boldsymbol{K}_{12} - \boldsymbol{K}_{21}) \boldsymbol{u}^e_{,\theta} + (\boldsymbol{K}_{13} - \boldsymbol{K}_{31}) \boldsymbol{u}^e_{,z} - \\ \boldsymbol{K}_{22} \boldsymbol{u}^e_{,\theta\theta} - (\boldsymbol{K}_{23} + \boldsymbol{K}_{32}) \boldsymbol{u}^e_{,\theta z} - \boldsymbol{K}_{33} \boldsymbol{u}^e_{,zz} - \\ \boldsymbol{K}^e_{01} \boldsymbol{T}^e + \boldsymbol{K}^e_{02} \boldsymbol{T}^e_{,\theta} + \boldsymbol{K}^e_{03} \boldsymbol{T}^e_{,z} \end{bmatrix} d\theta \, dz \, dt. \tag{14}$$

The second term in (13) is

$$\int_{t_0}^{t_1} \int_V \delta \boldsymbol{T'}^T \boldsymbol{K} \boldsymbol{T'} \, dV \, dt = \int_{t_0}^{t_1} \int_V (\delta \boldsymbol{T}^{eT} \boldsymbol{B}_1^T + \delta \boldsymbol{T}^{eT}_{,\theta} \boldsymbol{B}_2^T + \delta \boldsymbol{T}^{eT}_{,z} \boldsymbol{B}_3^T) \boldsymbol{K} (\boldsymbol{B}_1 \boldsymbol{T}^e + \boldsymbol{B}_2 \boldsymbol{T}^e_{,\theta} + \boldsymbol{B}_3 \boldsymbol{T}^e_{,z}) \, dV \, dt$$

$$= \int_{t_0}^{t_1} \int_z \int_\theta \delta \boldsymbol{T}^{eT} (\boldsymbol{g}_{11} \boldsymbol{T}^e - \boldsymbol{g}_{22} \boldsymbol{T}^e_{,\theta\theta} - \boldsymbol{g}_{33} \boldsymbol{T}^e_{,zz}) \, d\theta \, dz \, dt. \tag{15}$$

The third term in (13) is

$$\int_{t_0}^{t_1} \int_V \delta \boldsymbol{T'}^T (\boldsymbol{q} + \tau_0 \dot{\boldsymbol{q}}) \, dV \, dt = -\int_{t_0}^{t_1} \int_V \delta \boldsymbol{T}^T (\nabla \cdot \boldsymbol{q} + \tau_0 \nabla \cdot \dot{\boldsymbol{q}}) \, dV \, dt$$

$$= \int_{t_0}^{t_1} \int_V \delta \boldsymbol{T}^T (T_0 \rho \dot{\eta} + Q + \tau_0 T_0 \rho \ddot{\eta} + \tau_0 \dot{Q}) \, dV \, dt$$

$$= \int_{t_0}^{t_1} \int_V \delta \boldsymbol{T}^T \left(T_0 \boldsymbol{\beta}^T \dot{\boldsymbol{\varepsilon}} + \rho C_E \dot{T} + Q + \tau_0 (T_0 \boldsymbol{\beta}^T \ddot{\boldsymbol{\varepsilon}} + \rho C_E \ddot{T} + \dot{Q})\right) dV \, dt \tag{16}$$

$$= \int_{t_0}^{t_1} \int_z \int_\theta \delta \boldsymbol{T}^{eT} \begin{bmatrix} (\boldsymbol{f}_1 \dot{\boldsymbol{u}}^e + \boldsymbol{f}_2 \dot{\boldsymbol{u}}^e_{,\theta} + \boldsymbol{f}_3 \dot{\boldsymbol{u}}^e_{,z} + \boldsymbol{m}_0 \dot{\boldsymbol{T}}^e) + \\ \tau_0 (\boldsymbol{f}_1 \ddot{\boldsymbol{u}}^e + \boldsymbol{f}_2 \ddot{\boldsymbol{u}}^e_{,\theta} + \boldsymbol{f}_3 \ddot{\boldsymbol{u}}^e_{,z} + \boldsymbol{m}_0 \ddot{\boldsymbol{T}}^e) + \boldsymbol{Q}^e \end{bmatrix} d\theta \, dz \, dt.$$

The right-hand side of (13) has the form

$$\int_{t_0}^{t_1} \int_V \delta \boldsymbol{u}^T (\boldsymbol{f} - \rho \ddot{\boldsymbol{u}}) \, dV \, dt = \int_{t_0}^{t_1} \int_z \int_\theta \delta \boldsymbol{u}^{eT} (\boldsymbol{f}^e - \boldsymbol{M} \ddot{\boldsymbol{u}}^e) \, d\theta \, dz \, dt. \tag{17}$$

The element matrices appearing in equations (14)–(17) are defined in the Appendix. Equating the coefficients of $\delta \boldsymbol{u}^e$ in (13) to zero gives the equation

$$\boldsymbol{M} \ddot{\boldsymbol{u}}^e + \boldsymbol{K}_{11} \boldsymbol{u}^e - \boldsymbol{K}_{01} \boldsymbol{T}^e + (\boldsymbol{K}_{12} - \boldsymbol{K}_{21}) \boldsymbol{u}^e_{,\theta} + \boldsymbol{K}_{02} \boldsymbol{T}^e_{,\theta}$$
$$+ (\boldsymbol{K}_{13} - \boldsymbol{K}_{31}) \boldsymbol{u}^e_{,z} + \boldsymbol{K}_{03} \boldsymbol{T}^e_{,z} - \boldsymbol{K}_{22} \boldsymbol{u}^e_{,\theta\theta} - (\boldsymbol{K}_{23} + \boldsymbol{K}_{32}) \boldsymbol{u}^e_{,\theta z} - \boldsymbol{K}_{33} \boldsymbol{u}^e_{,zz} = \boldsymbol{f}^e. \tag{18}$$

Similarly, equating the coefficients of $\delta \boldsymbol{T}^e$ in (13) yields

$$\tau_0 \boldsymbol{f}_1 \ddot{\boldsymbol{u}}^e + \tau_0 \boldsymbol{m}_0 \ddot{\boldsymbol{T}}^e + \tau_0 \boldsymbol{f}_2 \ddot{\boldsymbol{u}}^e_{,\theta} + \tau_0 \boldsymbol{f}_3 \ddot{\boldsymbol{u}}^e_{,z} + \boldsymbol{m}_0 \dot{\boldsymbol{T}}^e + \boldsymbol{f}_1 \dot{\boldsymbol{u}}^e + \boldsymbol{f}_2 \dot{\boldsymbol{u}}^e_{,\theta} + \boldsymbol{f}_3 \dot{\boldsymbol{u}}^e_{,z} + \boldsymbol{g}_{11} \boldsymbol{T}^e - \boldsymbol{g}_{22} \boldsymbol{T}^e_{,\theta\theta} - \boldsymbol{g}_{33} \boldsymbol{T}^e_{,zz} = \boldsymbol{Q}^e. \tag{19}$$

Combining (18) and (19) and assembling the element matrices into global matrices leads to the governing equations of motion

$$\boldsymbol{H}_1\ddot{\boldsymbol{V}} + \boldsymbol{H}_2\ddot{\boldsymbol{V}}_{,\theta} + \boldsymbol{H}_3\ddot{\boldsymbol{V}}_{,z} + \boldsymbol{H}_4\dot{\boldsymbol{V}} + \boldsymbol{H}_5\dot{\boldsymbol{V}}_{,\theta} + \boldsymbol{H}_6\dot{\boldsymbol{V}}_{,z} + \boldsymbol{H}_7\boldsymbol{V} + \boldsymbol{H}_8\boldsymbol{V}_{,\theta} + \boldsymbol{H}_9\boldsymbol{V}_{,z} + \boldsymbol{H}_{10}\boldsymbol{V}_{,\theta\theta} + \boldsymbol{H}_{11}\boldsymbol{V}_{,\theta z} + \boldsymbol{H}_{12}\boldsymbol{V}_{,zz}$$
$$= \boldsymbol{F}, \quad (20)$$

where $\boldsymbol{H}_i$ ($i = 1, 2, \ldots, 12$) are the global matrices, given in the Appendix, $\boldsymbol{V}$ is the global nodal displacement and temperature vector, and $\boldsymbol{F}$ is a load vector defined by

$$\boldsymbol{F} = \begin{bmatrix} \boldsymbol{f}^e \\ \boldsymbol{Q}^e \end{bmatrix}. \quad (21)$$

The traction-free boundary conditions on surfaces of the cylinder require that the stresses at the inner and outer surfaces of the cylinder are zero:

$$\sigma_{rr} = \sigma_{r\theta} = \sigma_{rz} = 0 \quad \text{at} \quad r = r_i \text{ and } r = r_o. \quad (22)$$

The thermal boundary conditions are considered as

$$T_{,r} = 0 \quad \text{at} \quad r = r_i \text{ and } r = r_o. \quad (23)$$

These thermal boundary conditions imply that heat does not flow into or out of the system via the boundaries. Note that for a free cylinder without body forces and heat sources the right-hand side of (20) will be zero. Then, the homogeneous equation (20) leads to the eigenvalue problem for the determination of the dispersion relation between the frequency ω and the z-direction wave number k for a fixed circumferential integral wave number n. This was studied in [Chitikireddy et al. 2010].

3. Solution procedure for steady-state loading

In (20), the force vector $\boldsymbol{F}$ and the response $\boldsymbol{V}$ are assumed to be time harmonic with frequency ω. The θ-dependence of the load and response can be expressed in Fourier series as:

$$\boldsymbol{F}(\theta, z, t) = e^{-i\omega t}\boldsymbol{F}(\theta, z) = e^{-i\omega t}\sum_{n=-\infty}^{n=+\infty}\boldsymbol{F}_n(z)e^{in\theta},$$
$$\boldsymbol{V}(\theta, z, t) = e^{-i\omega t}\boldsymbol{V}(\theta, z) = e^{-i\omega t}\sum_{n=-\infty}^{n=+\infty}\boldsymbol{V}_n(z)e^{in\theta}. \quad (24)$$

Substitution of (24) into (20) yields a system of ordinary differential equations with Fourier coefficients $\boldsymbol{V}_n$ in terms of z. For each circumferential wave number (n), we obtain

$$\boldsymbol{H}_{12}\boldsymbol{V}_{n,zz} + (-\omega^2\boldsymbol{H}_3 - i\omega\boldsymbol{H}_6 + \boldsymbol{H}_9 + in\boldsymbol{H}_{11})\boldsymbol{V}_{n,z}$$
$$- [\omega^2(\boldsymbol{H}_1 + in\boldsymbol{H}_2) + i\omega(\boldsymbol{H}_4 + in\boldsymbol{H}_5) - (\boldsymbol{H}_7 + in\boldsymbol{H}_8 - n^2\boldsymbol{H}_{10})]\boldsymbol{V}_n = \boldsymbol{F}_n. \quad (25)$$

The following Fourier integral transform pairs are used to treat the z-dependence in (25):

$$\bar{\boldsymbol{V}}_n(k_n) = \int_{-\infty}^{+\infty}\boldsymbol{V}_n(z)e^{-ik_nz}\,dz, \quad \boldsymbol{V}_n(z) = \frac{1}{2\pi}\int_{-\infty}^{+\infty}\bar{\boldsymbol{V}}_n(k_n)e^{ik_nz}\,dk_n. \quad (26)$$

Application of Fourier transformation to (25) yields an algebraic equation in terms of the transform parameter (k_n):

$$-k_n^2 \mathbf{H}_{12}\bar{\mathbf{V}}_n + k_n \mathbf{H}_B \bar{\mathbf{V}}_n + \mathbf{H}_A \bar{\mathbf{V}}_n = \bar{\mathbf{F}}_n, \tag{27}$$

where

$$\mathbf{H}_B = -i\omega^2 \mathbf{H}_3 + \omega \mathbf{H}_6 + i\mathbf{H}_9 - n\mathbf{H}_{11},$$
$$\mathbf{H}_A = -\omega^2(\mathbf{H}_1 + in\mathbf{H}_2) - i\omega(\mathbf{H}_4 + in\mathbf{H}_5) + (\mathbf{H}_7 + in\mathbf{H}_8 - n^2\mathbf{H}_{10}).$$

Equation (27) is the governing equation for the n-th circumferential harmonic in the transformed domain.

The solution of (27) will be obtained in the form of an expansion in guided wave modes in the z-direction. For this purpose, we consider the homogeneous equation, which is a three-parameter algebraic eigensystem in ω, n, and k_n. If k_n serves as an eigenvalue for given values of ω and n, (27) gives a quadratic eigenvalue problem. Equation (27) can be converted into two first-order equations in the form

$$\begin{bmatrix} 0 & I \\ \mathbf{H}_A & \mathbf{H}_B \end{bmatrix} \begin{Bmatrix} \bar{\mathbf{V}}_n \\ k_n \bar{\mathbf{V}}_n \end{Bmatrix} - k_n \begin{bmatrix} I & 0 \\ 0 & \mathbf{H}_{12} \end{bmatrix} \begin{Bmatrix} \bar{\mathbf{V}}_n \\ k_n \bar{\mathbf{V}}_n \end{Bmatrix} = \begin{bmatrix} 0 \\ \bar{\mathbf{F}}_n \end{bmatrix}, \tag{28}$$

which we rewrite more compactly as

$$[\mathbf{A} - k_n \mathbf{B}]\mathbf{U}_n = \mathbf{P}_n. \tag{29}$$

If the displacement and temperature vector $\bar{\mathbf{V}}_n$ has dimension M, the dimension of $\mathbf{U}_n$ in (29) is $2M$. A nontrivial solution to the homogeneous form of (29) in terms of k_n yields $2M$ roots, denoted by k_{nm}. They represent axial wave numbers which can be real, purely imaginary, or complex. A real wave number represents a propagating wave and purely imaginary or complex wave numbers represent nonpropagating (evanescent) waves.

Once the wavenumbers and wave functions are found from (29), the response due to the n-th circumferential mode in the Fourier series representation of the applied loads can be obtained by modal summation. Associated with each eigenvalue there are right and left eigenvectors, $\mathbf{\Phi}_{nm}^R$ and $\mathbf{\Phi}_{nm}^L$, respectively, and they satisfy the equations

$$[\mathbf{A} - k_n \mathbf{B}]\mathbf{\Phi}_{nm}^R = 0, \quad [\mathbf{A}^T - k_n \mathbf{B}^T]\mathbf{\Phi}_{nm}^L = 0. \tag{30}$$

The right and left eigenvectors also satisfy the biorthogonality relations

$$\mathbf{\Phi}_{nm}^{L^T} \mathbf{B} \mathbf{\Phi}_{np}^R = \mathrm{diag}(B_{nm}), \quad \mathbf{\Phi}_{nm}^{L^T} \mathbf{A} \mathbf{\Phi}_{np}^R = \mathrm{diag}(k_{nm}B_{nm}), \tag{31}$$

where diag( ) denotes a diagonal matrix. The eigenvectors can also be partitioned into the following upper and lower halves (represented by subscript u and l, respectively):

$$\mathbf{\Phi}_{nm}^R = \begin{bmatrix} \mathbf{\Phi}_{nm\mathrm{u}}^R \\ \mathbf{\Phi}_{nm\mathrm{l}}^R \end{bmatrix}, \quad \mathbf{\Phi}_{nm}^L = \begin{bmatrix} \mathbf{\Phi}_{nm\mathrm{u}}^L \\ \mathbf{\Phi}_{nm\mathrm{l}}^L \end{bmatrix}. \tag{32}$$

The solution of (29) is expressed by summation of right eigenvectors as

$$\mathbf{U}_n = \sum_{m=1}^{2M} U_{nm}\mathbf{\Phi}_{nm}^R. \tag{33}$$

The coefficients U_{nm} are calculated by substituting (33) into (28) and using the biorthogonality relations (31). Then, the solution vector U_n is written as

$$U_n = \sum_{m=1}^{2M} \frac{\Phi_{mn}^{L^T} P_n}{(k_{nm} - k_n) B_{nm}} \Phi_{nm}^R. \tag{34}$$

The solution vector $\bar{V}_n$ in (28), occupying the upper half of U_n, takes the form

$$\bar{V}_n = \sum_{m=1}^{2M} \frac{\Phi_{mnl}^{L^T} \bar{F}_n}{(k_{nm} - k_n) B_{nm}} \Phi_{nmu}^R. \tag{35}$$

Inverse Fourier transform of (35) gives the response, $V_n(z)$, of the n-th circumferential harmonic in the spatial domain:

$$V_n(z) = \frac{1}{2\pi} \sum_{m=1}^{2M} \int_{-\infty}^{+\infty} \frac{\Phi_{mnl}^{L^T} \bar{F}_n}{(k_{nm} - k_n) B_{nm}} \Phi_{nmu}^R e^{ik_n z} \, dk_n. \tag{36}$$

In many problems, $\bar{F}_n$, Φ_{mn}^L, Φ_{nm}^R, and B_{nm} are independent of wave number k_n, so that application of the Cauchy residue theorem yields the modal response $V_n(z)$ in a straightforward way. The eigendata can be divided into two groups for travelling or decaying modes from the origin in $\pm z$ directions, respectively. Therefore, $V_n(z)$ can be expressed as summation of motions in the positive and negative directions as

$$V_n(z, \omega) = -i \sum_{m=1}^{M} \frac{\Phi_{mnl}^{L^T} \bar{F}_n}{B_{nm}} \Phi_{nmu}^R e^{ik_{nm} z} - i \sum_{m=M+1}^{2M} \frac{\Phi_{mnl}^{L^T} \bar{F}_n}{B_{nm}} \Phi_{nmu}^R e^{-ik_{nm} z}. \tag{37}$$

The response in the time domain is now obtained by applying an inverse Fourier transformation to (37) and is calculated numerically as

$$V_n(z, t) = \frac{1}{2\pi} \int_{-\infty}^{+\infty} V_n(z, \omega) e^{-i\omega t} \, d\omega. \tag{38}$$

4. Heat source representation

The heat input due to the laser pulse is assumed to be of the form

$$Q = I_0 f(t) \delta(\theta) g_r(r) g_z(z), \tag{39}$$

where I_0 is the energy of the laser pulse. The temporal profile $f(t)$ is assumed as

$$f(t) = \frac{t}{t_0^2} e^{-\frac{t}{t_0}}, \tag{40}$$

where t_0 is the pulse rise time. The spatial profile $g_z(z)$ is assumed to have a Gaussian profile in the z-direction,

$$g_z(z) = \frac{1}{\sqrt{\pi} a} e^{-z^2/a^2}, \tag{41}$$

where a is the radius of the laser beam. The depth dependence, $g_r(r)$, of the pulse is taken as

$$g_r(r) = \frac{\gamma}{r} e^{-\gamma(r_0 - r)}, \qquad (42)$$

where γ is the extinction coefficient. A schematic representation of the pulse and the frequency spectrum of $f(t)$ are shown in Figures 2 and 3, respectively. Here, the nondimensional frequency, $\omega^* = \omega H / \bar{v}$, where $\bar{v} = 2.5 \times 10^2$ m/s. Note that the rise time of the pulse, t_0, has been taken to be $1\,\mu$s.
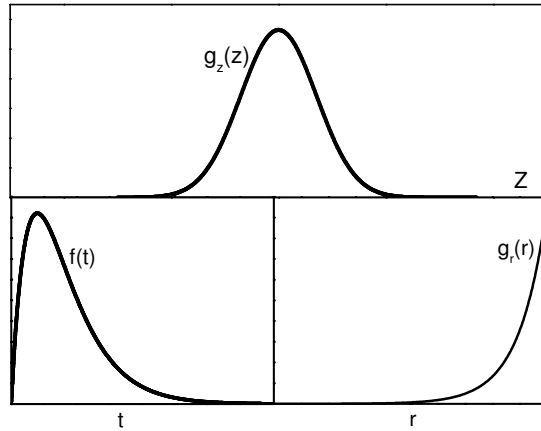
Figure 2. Temporal and spatial profiles of the pulse.
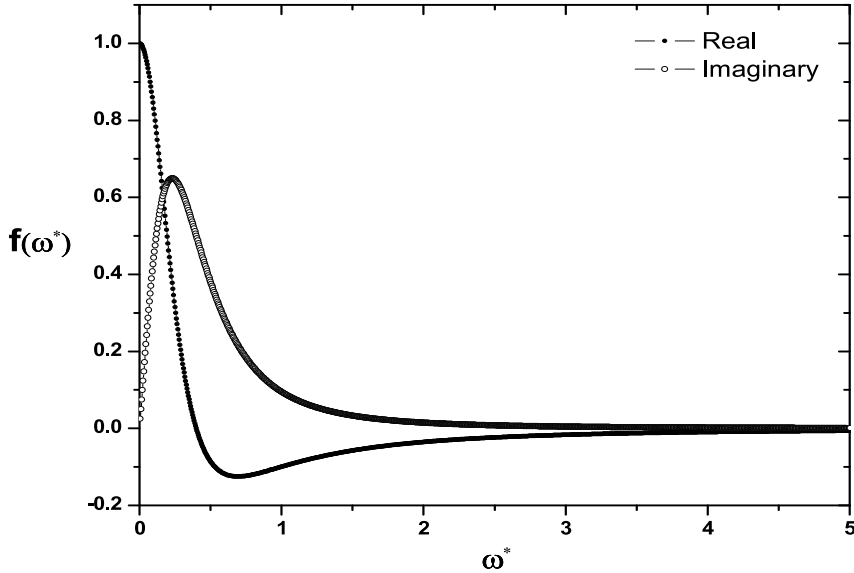
Figure 3. Frequency spectrum of $f(t)$.

Once the fundamental response functions $\boldsymbol{\Gamma}(z)$ are constructed due to $Q = I_0 f(t)\delta(\theta)g_r(r)\delta(z)$, the response due to the heat source Q, represented by (39), can be calculated as

$$\boldsymbol{v}(z_0) = \int_{-\infty}^{+\infty} \boldsymbol{\Gamma}(z)g_z(z - z_0)\, dz. \tag{43}$$

In the present work, only the thermal load is considered for constructing the response function. The spatial representation of the heat source along the radial profile in the frequency domain is

$$\boldsymbol{Q} = I_0 \bar{f}(\omega)\delta(\theta)\delta(z)\,\boldsymbol{Q}_0, \tag{44}$$

where $\boldsymbol{Q}_0 = (Q_1, Q_2, \ldots, Q_k, \ldots, Q_{2N+1})^T$ and Q_k is the value of $g_r(r)$ at the k-th node using a consistent load formulation. The solution procedure involves expansion of $\delta(\theta)$ in a Fourier series. It is well known that the Fourier series representation of a δ-function does not converge. Hence, it is necessary to replace the point source by a uniform spatial pulse of intensity q_0 over a circumferential distance $2r_0\theta_0$. For equivalence of a unit concentrated source, q_0 is given by

$$\int_{-\theta_0}^{+\theta_0} q_0 r_0 d\theta = 1 \quad \text{or} \quad q_0 = \frac{1}{2r_0\theta_0}. \tag{45}$$

Therefore, the θ-dependence of $\boldsymbol{Q}$ in (44) is represented by a Fourier series expansion in the circumferential direction as

$$\boldsymbol{Q} = \sum_{n=-\infty}^{n=+\infty} e^{in\theta}\,\boldsymbol{Q}_{n\theta}, \tag{46}$$

where

$$\boldsymbol{Q}_{n\theta} = \frac{1}{2\pi r_0}\frac{\sin n\theta_0}{n\theta_0} I_0 \bar{f}(\omega)\delta(z)\,\boldsymbol{Q}_0. \tag{47}$$

The Fourier transform of $\boldsymbol{Q}_{n\theta}$ in the z-direction is

$$\bar{\boldsymbol{Q}}_{n\theta} = \frac{1}{2\pi r_0}\frac{\sin n\theta_0}{n\theta_0} I_0 \bar{f}(\omega)\,\boldsymbol{Q}_0. \tag{48}$$

Since mechanical load is not considered here, the load vector in (27) becomes

$$\bar{\boldsymbol{F}}_n = \begin{bmatrix} 0 \\ \bar{\boldsymbol{Q}}_{n\theta} \end{bmatrix} = \frac{I_0 \bar{f}(\omega)}{2\pi r_0}\frac{\sin n\theta_0}{n\theta_0}\boldsymbol{F}_0, \tag{49}$$

where $\boldsymbol{F}_0 = \begin{bmatrix} 0 & \boldsymbol{Q}_0 \end{bmatrix}^T$. Substitution of (49) into (37) and considering propagation only in the $+z$ directions yields the n-th circumferential mode displacement and temperature response functions as

$$V_n(z, \omega) = \frac{-i\, I_0 \bar{f}(\omega)}{2\pi r_0}\frac{\sin n\theta_0}{n\theta_0}\sum_{m=1}^{M}\frac{\boldsymbol{\Phi}_{mnl}^{L^T}\boldsymbol{F}_0}{B_{nm}}\boldsymbol{\Phi}_{nmu}^{R}e^{ik_{nm}z}. \tag{50}$$

Using (50) in (46), we obtain

$$V(\theta, z, \omega) = \frac{-i\, I_0 \bar{f}(\omega)}{2\pi r_0}\sum_{n=-\infty}^{n=+\infty}\frac{\sin n\theta_0}{n\theta_0}e^{in\theta}\sum_{m=1}^{M}\frac{\boldsymbol{\Phi}_{mnl}^{L^T}\boldsymbol{F}_0}{B_{nm}}\boldsymbol{\Phi}_{nmu}^{R}e^{ik_{nm}z}. \tag{51}$$

Equation (51) is used in the next section to calculate the vector V at a given location (θ, z) for different frequencies ω. Attention is focused on the convergence of the numerical results by varying the number of nodes through the thickness of the cylinder, the number of terms $|n|$ in the Fourier series, and the number of modes M.

5. Numerical results and discussion

In this section, we consider propagation of thermoelastic waves in a cylindrical shell generated by the heat source represented by (39). The material of the cylinder is taken to be silicon nitride (Si_3N_4). Amorphous and textured Si_3N_4 has been widely studied in the past for its excellent mechanical properties, such as high resistance to thermal shock, resistance to chemical attack, high fracture toughness, and good tribological and wear properties. A good review of the processing and anisotropic properties of silicon nitride for various automotive and aerospace applications can be found in [Zhu and Sakka 2008] (see also [Kitayama et al. 1999; Vogelgesang et al. 2000; Yokota and Ibukiyama 2003]). Dispersion of thermoelastic guided waves in Si_3N_4 plates and cylindrical shells was reported in [Al-Qahtani and Datta 2004; Chitikireddy et al. 2010]. Here, we present results for the frequency dependent displacements, stresses, temperature, and thermal flux at an observation point due to the laser generated heating represented by (39).

We consider an infinite cylindrical tube with thickness 0.1 mm and inner radius 0.95 mm. Thus, the nondimensional inner and outer radii are $r_i = 9.5$ and $r_o = 10.5$. The shell is discretized into N equally

Quantity	Units	Silicon nitride
$\rho = \bar{\rho}$	kg/m^3	3.20×10^3
c_{11}	N/m^2	4.33×10^{11}
c_{12}	N/m^2	1.95×10^{11}
c_{13}	N/m^2	1.27×10^{11}
c_{33}	N/m^2	5.74×10^{11}
c_{44}	N/m^2	1.08×10^{11}
β_{rr}	N/m^2 °K	2.71×10^6
β_{zz}	N/m^2 °K	3.22×10^6
K_{rr}	W/m °K	43.5
$K_{zz} = \bar{k}$	W/m °K	55.4
c_E	J/kg °K	0.67×10^3
$T_0 = \bar{T}$	°K	296
τ_0	s	4.32×10^{-13}
a	μm	100
t_0	μs	1.0
H	mm	0.1
γ	m^{-1}	$1 \quad \times 10^5$
I_0	Nm	1.0
$\bar{c}$	N/m^2	$2 \quad \times 10^8$

Table 1. Thermomechanical properties of Si_3N_4.

thick coaxial circular cylinders, where N is allowed to take different values (25 and 50) in order to check for the convergence of the results. As discussed later, numerical results indicate that the heat flux in the radial direction, $|q_r|$, has sharp gradients near the inner and outer surfaces of the cylinder. So, numerical results are obtained also when the thickness is subdivided into 10 layers (5 at the outer end and 5 at the inner), each of thickness 0.00175 mm, and 25 layers of thickness 0.0033 mm each in the middle.

As mentioned above, the material of the cylinder is Si_3N_4, whose properties, from [Al-Qahtani and Datta 2004], are listed in Table 1. The symmetry axis of the material is aligned with the axis of the cylinder. The localized heat source is represented by (39) with $g_z(z)$ taken as $\delta(z)$. As noted before, once the response due to this source is known, that due to any other function $g_z(z)$ can be found by convolution; see (43). In the frequency domain, the frequency spectrum of $f(t)$ is shown in Figure 3. It is seen that the dominant contribution comes from the interval $0 \leq \omega^* \leq 5$, that is, the dominant frequency is between 0 and 1.99 MHz.

All the numerical results obtained here are in nondimensional forms. The nondimensional material properties of the tube are given by

$$\rho^* = 1.0, \qquad T_0^* = 1.0, \qquad \tau_0^* = 1.081 \times 10^{-6}, \qquad \beta_{rr}^* = 70.03, \qquad \beta_{\theta\theta}^* = 70.03,$$
$$\beta_{zz}^* = 83.21, \qquad k_{rr}^* = 0.785, \qquad k_{\theta\theta}^* = 0.785, \qquad k_{zz}^* = 1.00, \qquad c_E^* = 967.50. \tag{52}$$

The nondimensional elastic stiffness tensor is given by

$$C^* = \begin{bmatrix} 2165 & 975 & 635 & 0 & 0 & 0 \\ 975 & 2165 & 635 & 0 & 0 & 0 \\ 635 & 635 & 2870 & 0 & 0 & 0 \\ 0 & 0 & 0 & 540 & 0 & 0 \\ 0 & 0 & 0 & 0 & 540 & 0 \\ 0 & 0 & 0 & 0 & 0 & 765 \end{bmatrix}. \tag{53}$$

Dispersion curves for circumferential modes $n = 0$ are shown in Figure 4, and for $n = 1$ in Figure 5, where γ_R and γ_I are the real and imaginary parts of the wavenumber k_n^*. It is found that the elastic modes are not affected significantly by the thermal effects within the frequency range considered here. This is consistent with the findings reported in [Chitikireddy et al. 2010].

The computation of $V(\theta, z, \omega)$ using (51) involves two summations: one over the number of axial modes M for a fixed circumferential mode n and the other over circumferential modes n. The first is determined by the number of finite elements N_e used to discretize the thickness of the cylinder. The value of θ_0, appearing in (45), has been chosen as 0.01 radians. The observation location is at $\theta = \pi/4$ and $z = r_{mean}/4$. Furthermore, $g_z(z)$ is taken to be $\delta(z)$ and γ appearing in (42) is chosen as $105 \, \text{m}^{-1}$ (see Table 1).

To test the convergence of the series with the number of elements N_e for an appropriate choice of $|n|$, results were obtained for N_e as 15, 20, 35, and 50 keeping $|n|$ fixed at 50. The value of ω^* was taken as 5. Figure 6 shows the variation of displacement, temperature, stress, and radial heat flux through the thickness with the number N_e. It is seen that 35 elements are sufficient to assure convergence. It is interesting to note the variation of $|T|$ and $|q_r|$ through the thickness. The former decreases in a nearly linear manner from the boundaries towards the middle of the shell. Note the sharp change near the boundaries so that the slopes vanish at the boundaries to satisfy the zero heat flux conditions.
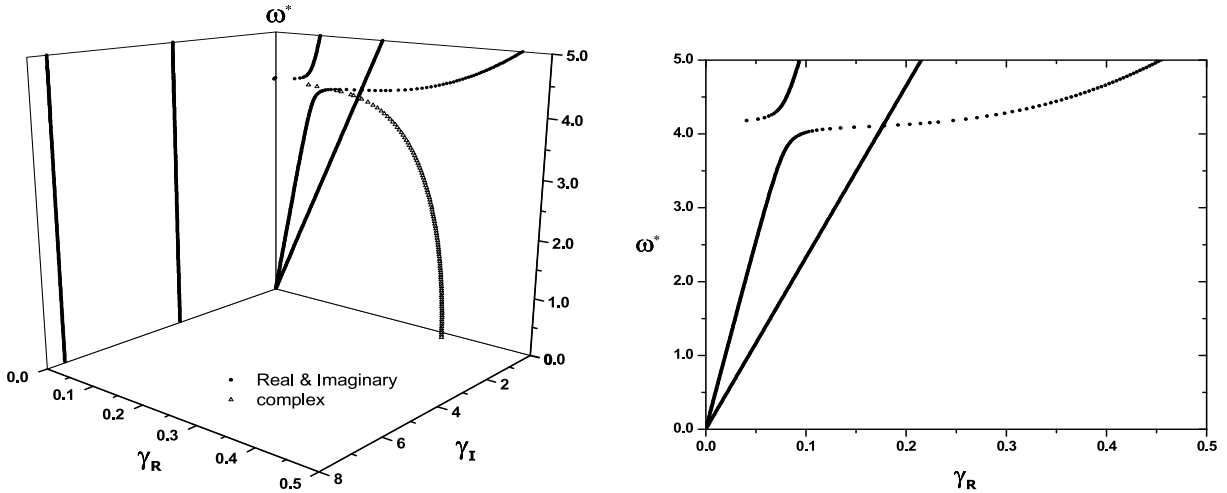
Figure 4. Frequency spectra of silicon nitride cylinder for $n = 0$. The two-dimensional diagram, corresponding to the plane $\gamma_I = 0$, shows the propagating (purely real) modes.
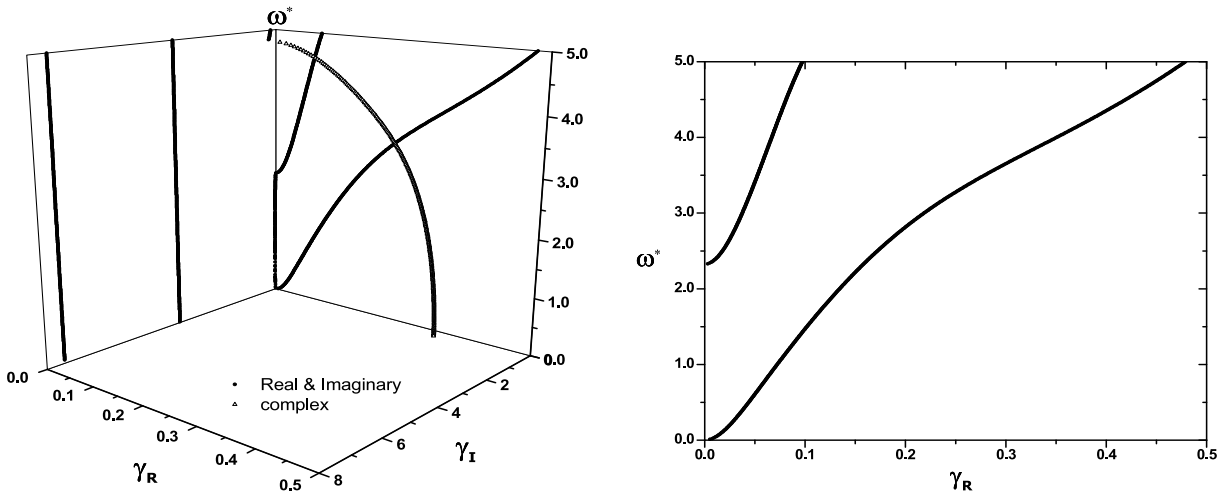
Figure 5. Frequency spectra of silicon nitride cylinder for $n = 1$. The two-dimensional diagram, corresponding to the plane $\gamma_I = 0$, shows the propagating (purely real) modes.

Consequently, the radial heat flux is nearly flat through most of the thickness and then drops steeply to zero at the boundaries. It is seen that convergence is achieved with both 35 and 50 elements.

Figures 7–9 show the changes in the distribution of the field quantities through the thickness at frequencies $\omega^* = 1, 3$, and 5. They also show variations with increasing $|n|$, which was assumed to take the values 20, 40, 50, and 60. The number of elements was kept at 35. It is seen that results converged when $|n|$ was 50. It is interesting to note that the rate of convergence increases with ω^*. This may be explained by noting the fact that the amplitudes decrease (because of diffusion) as the frequency increases. This is seen clearly in these figures.

Other features of these figures are as follows.
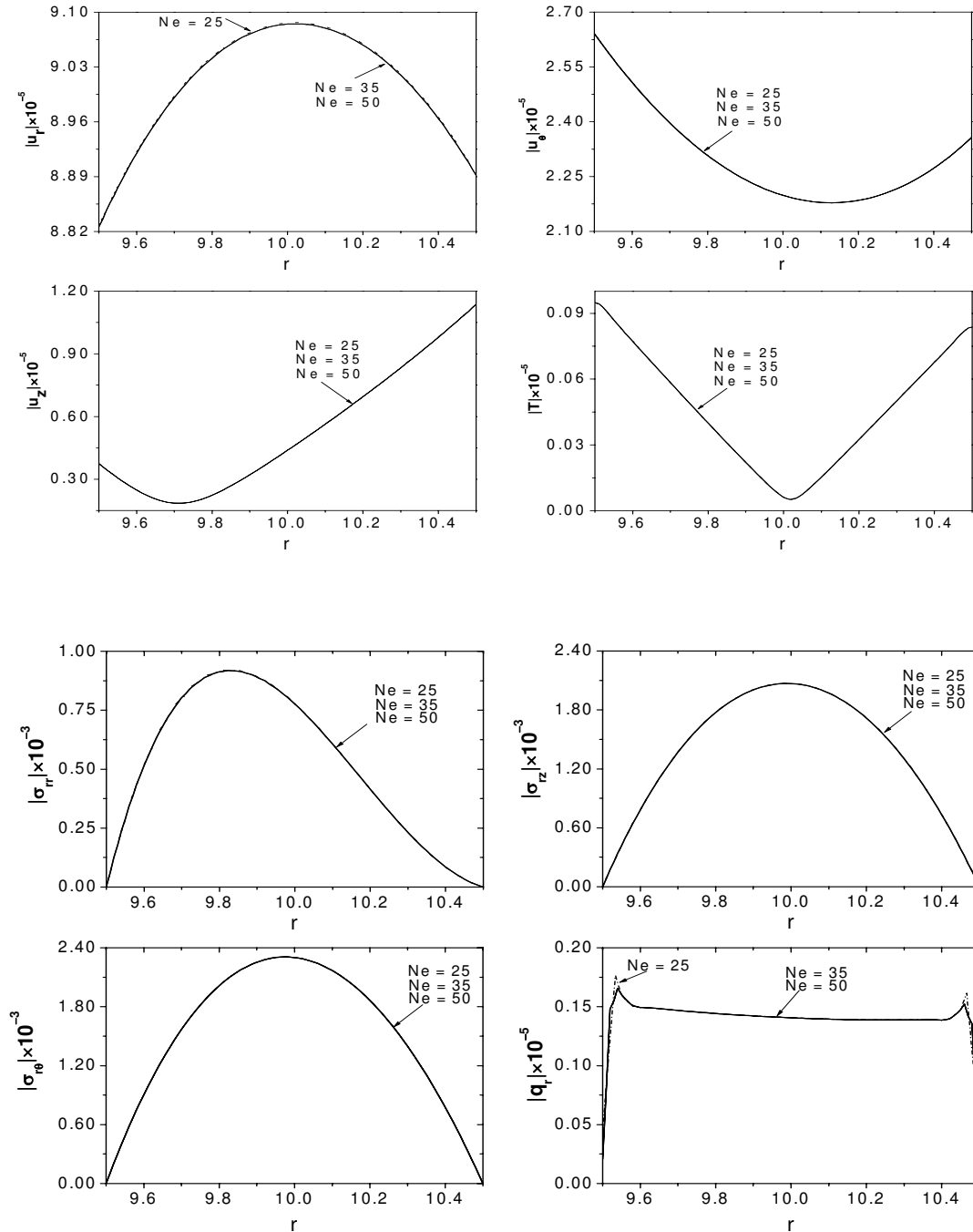
Figure 6. Through-the-thickness dependence of numerically calculated quantities for a silicon nitride cylinder at $\omega^* = 5.0$ with 25, 35, and 50 elements. The top two rows show the displacement components and the temperature distribution; the bottom two rows, the stress components and the heat flux.
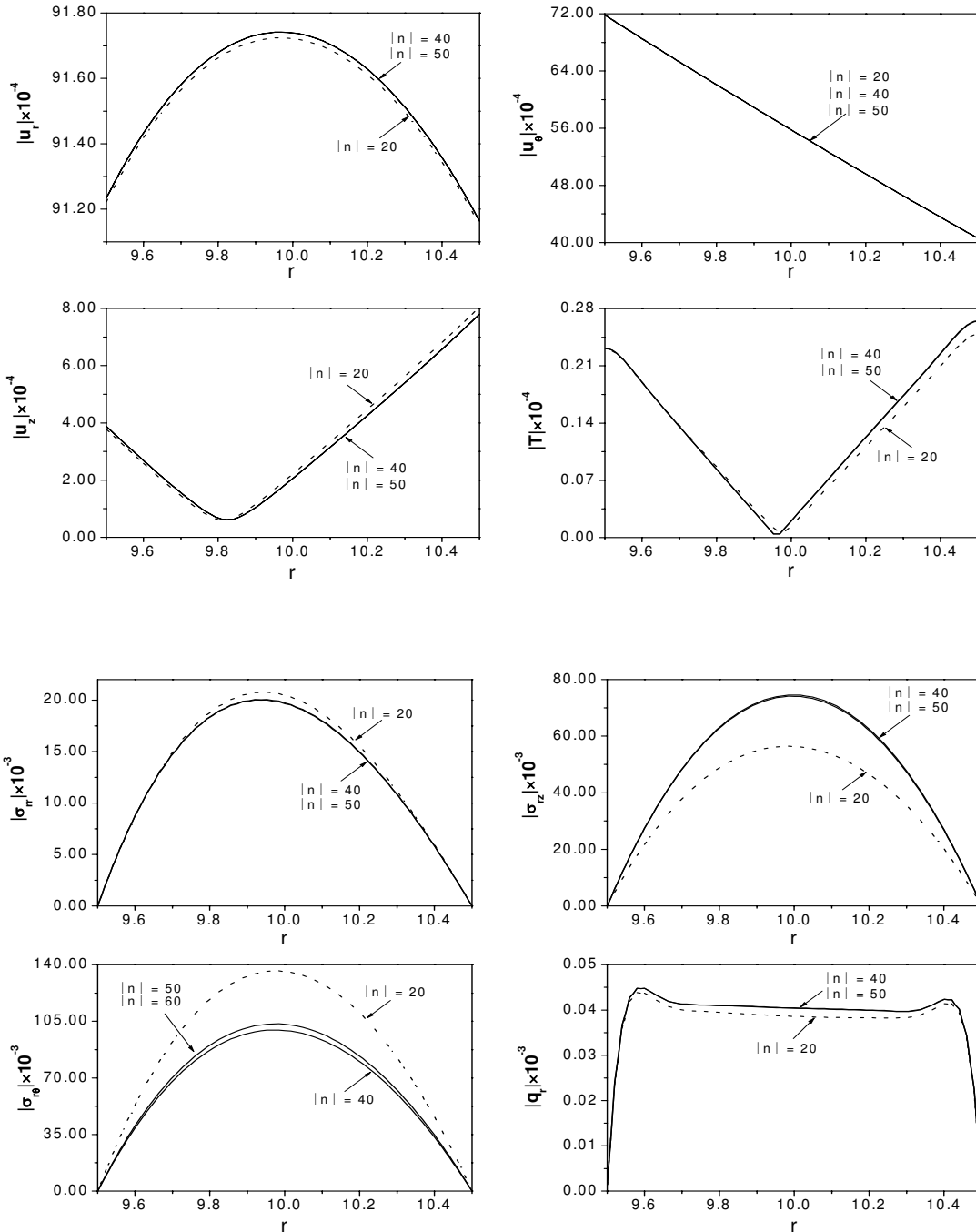
Figure 7. Through-the-thickness dependence of numerically calculated quantities for a silicon nitride cylinder at $\omega^* = 1.0$ with $|n| = 20$, 40, and 50. The top two rows show the displacement components and the temperature distribution; the bottom two rows, the stress components and the heat flux.
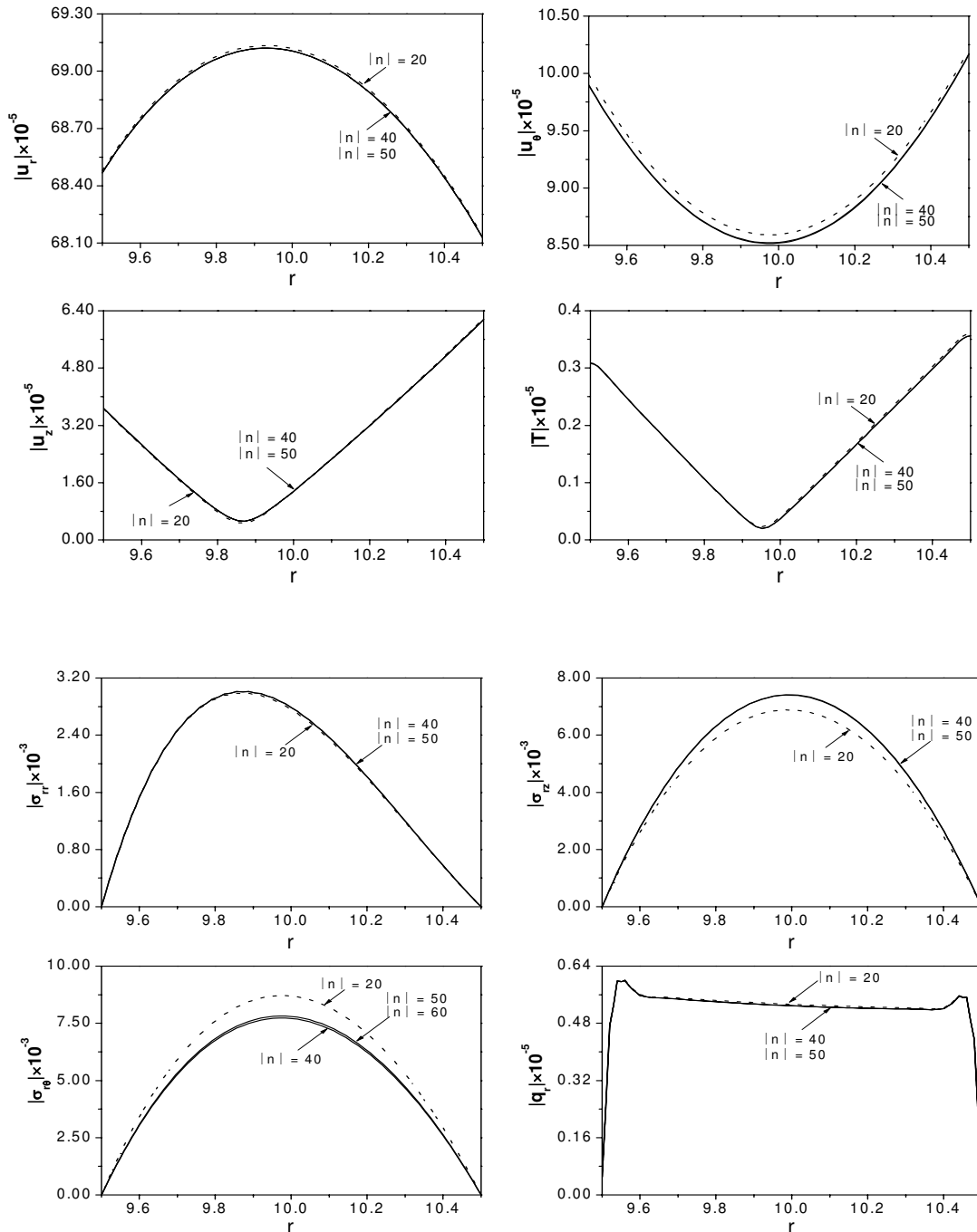
Figure 8. Through-the-thickness dependence of numerically calculated quantities for a silicon nitride cylinder at $\omega^* = 3.0$ with $|n| = 20$, 40, and 50. The top two rows show the displacement components and the temperature distribution; the bottom two rows, the stress components and the heat flux.
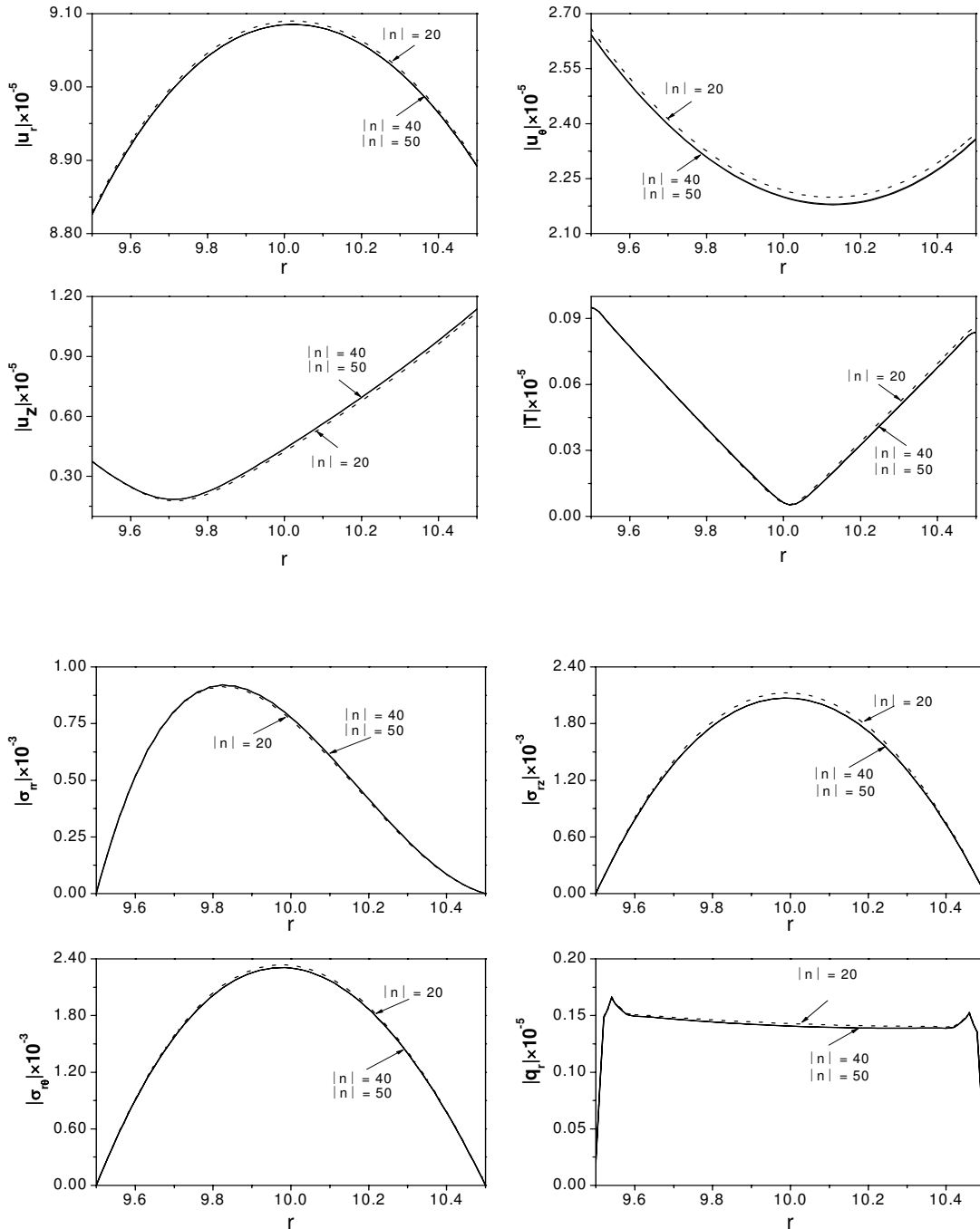
Figure 9. Through-the-thickness dependence of numerically calculated quantities for a silicon nitride cylinder at $\omega^* = 5.0$ with $|n| = 20$, 40, and 50. The top two rows show the displacement components and the temperature distribution; the bottom two rows, the stress components and the heat flux.

(1) At low frequencies, $|u_\theta|$ decreases in a linear fashion from the inner to the outer surface. As the frequency increases, it decreases first from the inner surface, reaches a minimum, and then increases with increasing radius. Both $|u_z|$ and $|T|$ also decrease first starting from the inner surface and then increase as the radius increases. The former attains the highest value at the outer surface, whereas the latter has the highest value at the outer surface at low frequencies; this feature is reversed at high frequencies.

(2) The radial displacement component and all the traction components increase from the inner surface (the latter being zero at both boundaries), reach maxima, and then decrease as the radius increases.

(3) Radial heat flux has the distinctive feature that it increases steeply from zero at the inner surface, reaches a plateau (slightly sloping towards the outer surface), and then decreases steeply to zero.

6. Conclusion

Propagation of thermoelastic waves in a circular cylindrical shell excited by a concentrated heat input has been studied in this paper. The generalized thermoelasticity theory developed by Lord and Shulman has been adopted. This theory includes a single thermal relaxation time. The material of the cylinder has been taken to be transversely isotropic Si_3N_4 as an illustrative example. However, the semianalytical finite element (SAFE) method that has been used here can also be used for generally anisotropic materials.

The heat input resembles that due to heating by a pulsed laser. It is focused at $r = r_o$, $\theta = 0$, $z = 0$, with a radial dependence that decays with decreasing r and acts on a small circular arc $2r_o\theta_0$, where $\theta_0 = .01$ radians. The solution can then be used for more general dependence on z and θ.

Although the solution presented here is for a concentrated heat source only, a concentrated mechanical load can easily be incorporated in the SAFE computations. This will be communicated in a future paper.

The results presented here are for discrete frequencies and the emphasis is on a study of convergence and distribution of the field quantities over the thickness of the cylinder. However, transient wave forms can be obtained by converting the continuous frequency spectrum using an inverse Fourier transform.

Appendix

$$
\boldsymbol{B}_1 = \begin{bmatrix} n_{1,r} & n_{2,r} & n_{3,r} \\ 0 & 0 & 0 \\ 0 & 0 & 0 \end{bmatrix}, \quad
\boldsymbol{B}_2 = \begin{bmatrix} 0 & 0 & 0 \\ \dfrac{n_1}{r} & \dfrac{n_2}{r} & \dfrac{n_3}{r} \\ 0 & 0 & 0 \end{bmatrix}, \quad
\boldsymbol{B}_3 = \begin{bmatrix} 0 & 0 & 0 \\ 0 & 0 & 0 \\ n_1 & n_2 & n_3 \end{bmatrix},
$$

$$
\boldsymbol{D}_1 = \begin{bmatrix}
n_{1,r} & 0 & 0 & n_{2,r} & 0 & 0 & n_{3,r} & 0 & 0 \\
\dfrac{n_1}{r} & 0 & 0 & \dfrac{n_2}{r} & 0 & 0 & \dfrac{n_3}{r} & 0 & 0 \\
0 & 0 & 0 & 0 & 0 & 0 & 0 & 0 & 0 \\
0 & 0 & 0 & 0 & 0 & 0 & 0 & 0 & 0 \\
0 & 0 & n_{1,r} & 0 & 0 & n_{2,r} & 0 & 0 & n_{3,r} \\
0 & n_{1,r} - \dfrac{n_1}{r} & 0 & 0 & n_{2,r} - \dfrac{n_2}{r} & 0 & 0 & n_{3,r} - \dfrac{n_3}{r} & 0
\end{bmatrix},
$$

$$\boldsymbol{D}_2 = \begin{bmatrix} 0 & 0 & 0 & 0 & 0 & 0 & 0 & 0 & 0 \\ 0 & \dfrac{n_1}{r} & 0 & 0 & \dfrac{n_2}{r} & 0 & 0 & \dfrac{n_3}{r} & 0 \\ 0 & 0 & 0 & 0 & 0 & 0 & 0 & 0 & 0 \\ 0 & 0 & \dfrac{n_1}{r} & 0 & 0 & \dfrac{n_2}{r} & 0 & 0 & \dfrac{n_3}{r} \\ 0 & 0 & 0 & 0 & 0 & 0 & 0 & 0 & 0 \\ \dfrac{n_1}{r} & 0 & 0 & \dfrac{n_2}{r} & 0 & 0 & \dfrac{n_3}{r} & 0 & 0 \end{bmatrix}, \quad \boldsymbol{D}_3 = \begin{bmatrix} 0 & 0 & 0 & 0 & 0 & 0 & 0 & 0 & 0 \\ 0 & 0 & 0 & 0 & 0 & 0 & 0 & 0 & 0 \\ 0 & 0 & n_1 & 0 & 0 & n_2 & 0 & 0 & n_3 \\ 0 & n_1 & 0 & 0 & n_2 & 0 & 0 & n_3 & 0 \\ n_1 & 0 & 0 & n_2 & 0 & 0 & n_3 & 0 & 0 \\ 0 & 0 & 0 & 0 & 0 & 0 & 0 & 0 & 0 \end{bmatrix},$$

$$\boldsymbol{K}_{jk} = \int_r \boldsymbol{D}_j^T \boldsymbol{C} \boldsymbol{D}_k r \, dr \quad (j, k = 1, 2, 3), \qquad \boldsymbol{K}_{0k} = \int_r \boldsymbol{D}_j^T \boldsymbol{\beta} \boldsymbol{N}_2 r \, dr \quad (k = 1, 2, 3),$$

$$\boldsymbol{M} = \int_r \rho \boldsymbol{N}_1^T \boldsymbol{N}_1 r \, dr, \qquad \boldsymbol{g}_{jj} = \int_r \boldsymbol{B}_j^T \boldsymbol{K} \boldsymbol{B}_j r \, dr \quad (j = 1, 2, 3),$$

$$\boldsymbol{f}_j = \int_r T_0 \boldsymbol{N}_2^T \boldsymbol{\beta}^T \boldsymbol{D}_j r \, dr \quad (j = 1, 2, 3), \qquad \boldsymbol{m}_0 = \int_r \rho c_E \boldsymbol{N}_2^T \boldsymbol{N}_2 r \, dr, \qquad \boldsymbol{f}^e = \int_r \boldsymbol{N}_2^T \boldsymbol{f} r \, dr,$$

$$\boldsymbol{H}_1 = \begin{bmatrix} \boldsymbol{M} & 0 \\ \tau_0 \boldsymbol{f}_1 & \tau_0 \boldsymbol{m}_0 \end{bmatrix}, \quad \boldsymbol{H}_2 = \begin{bmatrix} 0 & 0 \\ \tau_0 \boldsymbol{f}_2 & 0 \end{bmatrix}, \quad \boldsymbol{H}_3 = \begin{bmatrix} 0 & 0 \\ \tau_0 \boldsymbol{f}_3 & 0 \end{bmatrix}, \quad \boldsymbol{H}_4 = \begin{bmatrix} 0 & 0 \\ \boldsymbol{f}_1 & \boldsymbol{m}_0 \end{bmatrix}, \quad \boldsymbol{H}_5 = \begin{bmatrix} 0 & 0 \\ \boldsymbol{f}_2 & 0 \end{bmatrix},$$

$$\boldsymbol{H}_6 = \begin{bmatrix} 0 & 0 \\ \boldsymbol{f}_3 & 0 \end{bmatrix}, \quad \boldsymbol{H}_7 = \begin{bmatrix} \boldsymbol{K}_{11} & -\boldsymbol{K}_{01} \\ 0 & \boldsymbol{g}_{11} \end{bmatrix}, \quad \boldsymbol{H}_8 = \begin{bmatrix} \boldsymbol{K}_{12} - \boldsymbol{K}_{21} & \boldsymbol{K}_{02} \\ 0 & 0 \end{bmatrix}, \quad \boldsymbol{H}_9 = \begin{bmatrix} \boldsymbol{K}_{13} - \boldsymbol{K}_{31} & \boldsymbol{K}_{03} \\ 0 & 0 \end{bmatrix},$$

$$\boldsymbol{H}_{10} = \begin{bmatrix} -\boldsymbol{K}_{22} & 0 \\ 0 & -\boldsymbol{g}_{22} \end{bmatrix}, \quad \boldsymbol{H}_{11} = \begin{bmatrix} -(\boldsymbol{K}_{23} + \boldsymbol{K}_{32}) & 0 \\ 0 & 0 \end{bmatrix}, \quad \boldsymbol{H}_{12} = \begin{bmatrix} -\boldsymbol{K}_{33} & 0 \\ 0 & -\boldsymbol{g}_{33} \end{bmatrix}.$$

References

[Al-Qahtani and Datta 2004] H. M. Al-Qahtani and S. K. Datta, "Thermoelastic waves in an anisotropic infinite plate", *J. Appl. Phys.* **96**:7 (2004), 3645–3658.

[Al-Qahtani et al. 2005] H. M. Al-Qahtani, S. K. Datta, and O. M. Mukdadi, "Laser-generated thermoelastic waves in an anisotropic infinite plate: FEM Analysis", *J. Thermal Str.* **28**:11 (2005), 1099–1122.

[Chitikireddy et al. 2010] R. Chitikireddy, H. Bai, A. H. Shah, and S. K. Datta, "Thermoelastic waves in an anisotropic cylinder", *J. Thermal Str.* **33**:2 (2010), 97–120.

[Clorennec and Royer 2003] D. Clorennec and D. Royer, "Analysis of surface acoustic wave propagation on a cylinder using laser ultrasonics", *Appl. Phys. Letters* **82**:25 (2003), 4608–4610.

[Datta and Shah 2009] S. K. Datta and A. H. Shah, *Elastic waves in composite media and structures: with applications to ultrasonic nondestructive evaluation*, CRC Press, 2009.

[Elnagar and Abd-Alla 1987] A. M. Elnagar and A. M. Abd-Alla, "On a generalized thermo-elastic problem in an infinite cylinder under initial stress", *Earth, Moon and Planets* **37**:3 (1987), 213–223.

[Erbay and Şuhubi 1986] S. Erbay and E. S. Şuhubi, "Longitudinal wave propagation in a generalized thermoelastic cylinder", *J. Thermal Str.* **9**:3 (1986), 279–295.

[Green and Lindsay 1972] A. E. Green and K. A. Lindsay, "Thermoelasticity", *J. Elast.* **2**:1 (1972), 1–7.

[Green and Naghdi 1993] A. E. Green and P. M. Naghdi, "Thermoelasticity without energy dissipation", *J. Elast.* **31**:3 (1993), 189–208.

[Ignaczak and Ostoja-Starzewski 2010] J. Ignaczak and M. Ostoja-Starzewski, *Thermoelasticity with finite wave speeds*, Oxford University Press, New York, 2010.

[Kitayama et al. 1999] M. Kitayama, K. Hirao, M. Toriyama, and S. Kanazaki, "Thermal conductivity of β-Si$_3$N$_4$, I: effects of various microstructural factors", *J. Amer. Ceram. Soc.* **82**:11 (1999), 3105–3112.

[Lord and Shulman 1967] H. W. Lord and Y. Shulman, "A generalized dynamical theory of thermoelasticity", *J. Mech. Phys. Solids* **15**:5 (1967), 299–309.

[Pan et al. 2004] Y. Pan, C. Rossignol, and B. Audoin, "Acoustic waves generated by a laser point source in an isotropic cylinder", *J. Acoust. Soc. Am.* **116**:2 (2004), 814–820.

[Pan et al. 2006] Y. Pan, M. Perton, B. Audoin, and C. Rossignol, "Acoustic waves generated by a laser point source in a transversely isotropic cylinder", *J. Acoust. Soc. Am.* **119**:1 (2006), 243–250.

[Ponnusamy 2007] P. Ponnusamy, "Wave propagation in a generalized thermoelastic solid cylinder of arbitrary cross-section", *Int. J. Solids Str.* **44**:16 (2007), 5336–5348.

[Scruby and Drain 1990] C. B. Scruby and L. E. Drain, *Laser ultrasonics: techniques and applications*, Adam Hilger, New York, 1990.

[Sharma 2001] J. N. Sharma, "Three-dimensional analysis of a homogeneous transversely isotropic thermoelastic cylindrical panel", *J. Acoust. Soc. Am.* **110**:1 (2001), 254–259.

[Sharma and Sharma 2002] J. N. Sharma and P. K. Sharma, "Free vibration analysis of homogeneous transversely isotropic thermoelastic cylindrical panel", *J. Thermal Str.* **25**:2 (2002), 169–182.

[Sharma et al. 2000] J. N. Sharma, R. Singh, and R. Kumar, "Generalized thermoelastic waves in homogeneous isotropic plates", *J. Acoust. Soc. Am.* **108**:2 (2000), 848–851.

[Verma 2002] K. L. Verma, "On the propagation of waves in layered anisotropic media in generalized thermoelasticity", *Internat. J. Engrg. Sci.* **40**:18 (2002), 2077–2096.

[Verma and Hasebe 2001] K. L. Verma and N. Hasebe, "Dispersion of thermoelastic waves in a plate with and without energy dissipation", *Int. J. Thermophys.* **22**:3 (2001), 957–978.

[Vogelgesang et al. 2000] R. Vogelgesang, M. Grimsditch, and J. S. Wallace, "The elastic constants of single crystal β-Si$_3$N$_4$", *Appl. Phys. Lett.* **76**:8 (2000), 982–984.

[Yokota and Ibukiyama 2003] H. Yokota and M. Ibukiyama, "Microstructure tailoring for high thermal conductivity of β-Si$_3$N$_4$ ceramics", *J. Amer. Ceram. Soc.* **86**:1 (2003), 197–199.

[Zhu and Sakka 2008] X. Zhu and Y. Sakka, "Textured silicon nitride: processing and anisotropic properties", *Sci. Technol. Adv. Mater.* **9**:3 (2008), 1–47.

[Zhuang et al. 1999] W. Zhuang, A. H. Shah, and S. B. Dong, "Elastodynamic green's function for laminated anisotropic circular cylinders", *J. Appl. Mech.* (*ASME*) **66**:3 (1999), 665–673.

HAO BAI: hbai@lakeheadu.ca
Department of Mechanical Engineering, Lakehead University, 955 Oliver Rd, Thunder Bay, ON P7B 5E1, Canada

RAVI CHITIKIREDDY: umchitik@cc.umanitoba.ca
Department of Civil Engineering, University of Manitoba, Winnipeg, MB R3T 2N2, Canada

ARVIND H. SHAH: shah@cc.umanitoba.ca
Department of Civil Engineering, University of Manitoba, Winnipeg, MB R3T 2N2, Canada

SUBHENDU K. DATTA: Subhendu.Datta@colorado.edu
Department of Mechanical Engineering, University of Colorado, Boulder, CO 80309-0427, United States